

## Research Article

# Near-Field Source Localization by Using Focusing Technique

Hongyang He, Yide Wang, and Joseph Saillard

*Ecole Polytechnique de l'Université de Nantes, Institut de Recherche en Electrotechnique et Electronique de Nantes Atlantique (IREENA), Rue Christian Pauc, BP 50609, 44306 Nantes Cedex 3, France*

Correspondence should be addressed to Hongyang He, hongyang.he@etu.univ-nantes.fr

Received 2 June 2008; Revised 30 September 2008; Accepted 7 November 2008

Recommended by M. Greco

We discuss two fast algorithms to localize multiple sources in near field. The symmetry-based method proposed by Zhi and Chia (2007) is first improved by implementing a search-free procedure for the reduction of computation cost. We present then a focusing-based method which does not require symmetric array configuration. By using focusing technique, the near-field signal model is transformed into a model possessing the same structure as in the far-field situation, which allows the bearing estimation with the well-studied far-field methods. With the estimated bearing, the range estimation of each source is consequently obtained by using 1D MUSIC method without parameter pairing. The performance of the improved symmetry-based method and the proposed focusing-based method is compared by Monte Carlo simulations and with Crammer-Rao bound as well. Unlike other near-field algorithms, these two approaches require neither high-computation cost nor high-order statistics.

Copyright © 2008 Hongyang He et al. This is an open access article distributed under the Creative Commons Attribution License, which permits unrestricted use, distribution, and reproduction in any medium, provided the original work is properly cited.

## 1. INTRODUCTION

In the last two decades, subspace-based methods for estimating the directions of arrival (DOA) of far-field sources impinging on an array of sensors have become very popular. In particular, the MUSIC algorithm [1] and its derivatives have received much attention [2]. Most of these methods make the assumption that the sources are located relatively far from the array so that the waves emitted by the sources can be considered as plane waves. With this assumption, each signal wavefront can be characterized by their DOA. However, when a source is located close to the array (i.e., near field), the wavefront must be characterized by both the azimuth and range. Methods based on the far-field assumption are no longer applicable to this situation. The near-field situation can occur, for example, in sonar, electronic surveillance, and seismic exploration.

Recently, many localization methods for near-field sources have been proposed, such as maximum likelihood method in [2, 3], the 2D MUSIC method in [2, 4], the model-fitting method in [5], the linear prediction method in [6], the higher-order ESPRIT method in [1, 7], and so forth. Most of these methods either involve multidimensional spectral peak search, or contain an additional parameters pairing procedure, or high-order statistics computation.

In order to reduce the computational complexity involved in most of the above algorithms, more recently, Zhi and Chia proposed a fast method based on symmetric array configuration in [8]. By applying Fresnel approximation, the received signal model in near field is first decomposed into a far-field part and a near-field part. Far-field-like rotational invariance property is found thanks to the symmetric structure of the arrays, which allows the bearing estimation by a search-based ESPRIT-like method. The range is obtained by implementing 1D MUSIC method for each estimated bearing.

In this paper, we first improve the symmetry-based method proposed in [8] by implementing a rooting procedure [9, 10]. The improved algorithm requires no longer spectral peak search for the bearing estimation. In the second part of this paper, we propose a focusing-based source localization approach for arbitrary ULAs. From the same received signal model as in [8], the near-field part of the received signal model is approximately eliminated by using focusing technique. Consequently, the far-field search-free DOA algorithms can be employed for the bearing estimation. The range is estimated by the same way as in [8] with the estimated bearings. Similar to the focusing technique in wide-band source localization [11], the focusing matrix is obtained from a beamforming-based pre-estimation which

is implemented with a rough 2D search. Therefore, the algorithm is implemented in four steps: (1) estimate an approximate location of the closely located sources with a beamforming-based method; (2) apply focusing to the covariance matrix of the received signal; (3) estimate the bearing of the sources with a far-field subspace-based method; (4) find the ranges of the sources by 1D MUSIC method with the estimated bearings. This algorithm does not require high-order statistics computation, parameter pairing or symmetric array configuration, in addition, it has high-resolution performance in contrast with other fast near-field methods.

The rest of this paper is organized as follows. Section 2 addresses the received signal model in near-field situation. Section 3 presents the bearing estimation methods in near field including the improvement of the method in [8] and the proposed focusing-based method. Range estimation is discussed in Section 4. The simulation results for performance testing of the proposed approach are shown in Section 5, and Section 6 concludes the whole paper.

## 2. NEAR-FIELD SIGNAL MODEL

### 2.1. Received signal model for ULA

Consider a near-field scenario of  $K$  uncorrelated narrow-band signals impinging to a  $2M + 1$ -element ULA as illustrated in Figure 1. Let the array center be the phase reference point. The received signal at the  $m$ th sensor can be modeled as

$$x_m(t) = \sum_{k=1}^K e^{j\tau_{mk}} s_k(t) + n_m(t), \quad (1)$$

where  $s_k(t)$  is the  $k$ th source signal received at the reference point,  $n_m(t)$  is an additive complex circular white Gaussian noise independent of signals, and  $\tau_{mk}$  is the phase shift associated with propagation time delay between the reference point and sensor  $m$  of the  $k$ th source signal, which is a function of source signal parameters, range  $r_k$ , angle  $\theta_k$ , and wavelength  $\lambda$ , given by

$$\tau_{mk} = \frac{2\pi}{\lambda} \left( \sqrt{r_k^2 + (md)^2} - 2r_k m d \sin \theta_k - r_k \right). \quad (2)$$

The received signal vector  $\mathbf{x}(t) = [x_{-M}(t), \dots, x_M(t)]^T$ , with the superscript  $T$  denoting matrix transposition, can be written as

$$\mathbf{x}(t) = \mathbf{A}\mathbf{s}(t) + \mathbf{n}(t), \quad (3)$$

where  $\mathbf{s}(t) = [s_1(t), \dots, s_K(t)]^T$  is the signal vector,  $\mathbf{n}(t) = [n_{-M}(t), \dots, n_M(t)]^T$  is the noise vector and  $\mathbf{A}$  is the array manifold matrix, given by

$$\mathbf{A} = [\mathbf{a}(r_1, \theta_1), \dots, \mathbf{a}(r_K, \theta_K)], \quad (4)$$

with the steering vector  $\mathbf{a}(r_k, \theta_k)$  being expressed as

$$\mathbf{a}(r_k, \theta_k) = \begin{bmatrix} a_{k,-M} \\ \vdots \\ a_{k,M} \end{bmatrix} = \begin{bmatrix} e^{j\tau_{-Mk}} \\ \vdots \\ e^{j\tau_{Mk}} \end{bmatrix}. \quad (5)$$

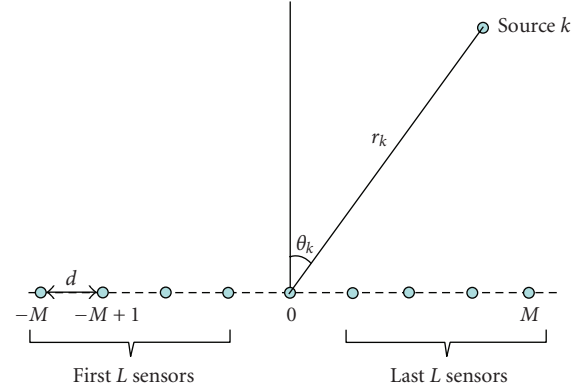


FIGURE 1: Source localization in near field with ULA.

### 2.2. Approximated model for symmetric ULA

By using the second-order Taylor expansion to (2), we have

$$\tau_{mk} = \left( -\frac{2\pi d}{\lambda} \sin \theta_k \right) m + \left( \frac{\pi d^2}{\lambda r_k} \cos^2(\theta_k) \right) m^2 + o\left(\frac{d^2}{r_k^2}\right), \quad (6)$$

where  $o(d^2/r_k^2)$  denotes the terms of order greater than  $d^2/r_k^2$ . By omitting the high-order terms approximately, the signal model can be written as

$$x_m(t) = \sum_{k=1}^K e^{j(-2\pi d/\lambda) \sin \theta_k m + j((\pi d^2/\lambda r_k) \cos^2(\theta_k)) m^2} s_k(t) + n_m(t). \quad (7)$$

Therefore, the steering vector  $\mathbf{a}(r_k, \theta_k)$  in (4) can be expressed as

$$\mathbf{a}(r_k, \theta_k) = \begin{bmatrix} e^{j(2\pi d/\lambda) \sin \theta_k M + j((\pi d^2/\lambda r_k) \cos^2(\theta_k)) M^2} \\ \vdots \\ e^{-j(2\pi d/\lambda) \sin \theta_k M + j((\pi d^2/\lambda r_k) \cos^2(\theta_k)) M^2} \end{bmatrix}. \quad (8)$$

Observing that the second terms of the elements in (8) are symmetric, we divide the ULA into two subarrays as shown in Figure 1. The first subarray is formed with the first  $L$  sensors (from sensor  $-M$  to sensor  $-M + L - 1$ ), and the second subarray is formed with the last  $L$  sensors (from sensor  $M - L + 1$  to sensor  $M$ ). The received signal vectors of the two subarrays can be written as

$$\begin{aligned} \mathbf{x}_1(t) &= [x_{-M}(t), x_{-M+1}(t), \dots, x_{-M+(L-1)}(t)]^T, \\ \mathbf{x}_2(t) &= [x_{M-(L-1)}(t), \dots, x_{M-1}(t), x_M(t)]^T, \end{aligned} \quad (9)$$

where  $K < L < 2M + 1$ . These two subarray vectors have similar forms as

$$\begin{aligned} \mathbf{x}_1(t) &= \mathbf{A}_1 \mathbf{s}(t) + \mathbf{n}_1(t), \\ \mathbf{x}_2(t) &= \mathbf{A}_2 \mathbf{s}(t) + \mathbf{n}_2(t), \end{aligned} \quad (10)$$

where  $\mathbf{n}_1(t) = [n_{-M}(t), \dots, n_{-M+(L-1)}(t)]^T$  and  $\mathbf{n}_2(t) = [n_{M-(L-1)}(t), \dots, n_M(t)]^T$  are subarray noise vectors. The

matrix  $\mathbf{A}_1$  is the first  $L$  rows of  $\mathbf{A}$ , and  $\mathbf{A}_2$  is constructed with the last  $L$  rows of  $\mathbf{A}$ .

The relationship between  $\mathbf{A}$ ,  $\mathbf{A}_1$ , and  $\mathbf{A}_2$  is

$$\mathbf{A} = \begin{bmatrix} \mathbf{A}_1 \\ \text{last } 2M+1-L \text{ rows} \end{bmatrix} = \begin{bmatrix} \text{first } 2M+1-L \text{ rows} \\ \mathbf{A}_2 \end{bmatrix}. \quad (11)$$

$\mathbf{A}_1$  is defined as

$$\mathbf{A}_1 = [\mathbf{a}_1(r_1, \theta_1), \dots, \mathbf{a}_1(r_K, \theta_K)], \quad (12)$$

with

$$\mathbf{a}_1(r_k, \theta_k) = \begin{bmatrix} e^{j((2\pi d/\lambda) \sin \theta_k)M + j((\pi d^2/\lambda r_k) \cos^2(\theta_k))M^2} \\ \vdots \\ e^{j((2\pi d/\lambda) \sin \theta_k)(M-L+1) + j((\pi d^2/\lambda r_k) \cos^2(\theta_k))((2\pi d/\lambda) \sin \theta_k)(M-L+1)^2} \end{bmatrix}. \quad (13)$$

The symmetric property implied in (8) gives

$$\mathbf{A}_2 = [\mathbf{D}(\theta_1)(\mathbf{J}\mathbf{a}_1(r_1, \theta_1)), \dots, \mathbf{D}(\theta_K)(\mathbf{J}\mathbf{a}_1(r_K, \theta_K))], \quad (14)$$

where  $\mathbf{J}$  is the anti-identity matrix and

$$\mathbf{D}(\theta_k) = \text{diag}[e^{j(-4\pi d/\lambda) \sin \theta_k(M-L+1)}, \dots, e^{j(-4\pi d/\lambda) \sin \theta_k M}]. \quad (15)$$

### 2.3. Covariance matrix of the received signal and eigen decomposition

The covariance matrix of the received signal can be written as

$$\mathbf{R}_x = E[\mathbf{x}(t)\mathbf{x}^H(t)] = \mathbf{A}\mathbf{R}_s\mathbf{A}^H + \sigma^2\mathbf{I}, \quad (16)$$

where the superscript  $H$  denotes matrix conjugate transposition,  $\sigma^2$  is the power of noise, and  $\mathbf{R}_s = E[\mathbf{s}(t)\mathbf{s}^H(t)]$  is the covariance matrix of the received signal at the reference point.

The eigen decomposition of the array covariance matrix yields

$$\mathbf{R}_x = \mathbf{U}_s\mathbf{\Lambda}_s\mathbf{U}_s^H + \mathbf{U}_n\mathbf{\Lambda}_n\mathbf{U}_n^H, \quad (17)$$

where  $\mathbf{U}_s \in C^{(2M+1) \times K}$  contains  $K$  eigenvectors spanning the signal subspace of  $\mathbf{R}_x$ , and the diagonal matrix  $\mathbf{\Lambda}_s \in C^{K \times K}$  contains the corresponding eigenvalues. Similarly,  $\mathbf{U}_n \in C^{(2M+1) \times (2M+1-K)}$  contains  $2M+1-K$  eigenvectors in the noise subspace of  $\mathbf{R}_x$ , and the diagonal matrix  $\mathbf{\Lambda}_n \in C^{(2M+1-K) \times (2M+1-K)}$  contains the corresponding eigenvalues.

## 3. NEAR-FIELD BEARING ESTIMATION

### 3.1. Improvement on the symmetry-based algorithm

From the symmetric array configuration, Zhi and Chia proposed in [8] a symmetry-based technique for near-field

bearing estimation. This estimator develops the symmetric property in the manifold matrix and has found a rank reduction-based algorithm to estimate the bearing. We note that the rank reduction-based method is first proposed in [10, 12] for the estimation of far-field DOAs, whereas the symmetry-based algorithm [8] develops the rank reduction property for near-field bearing estimation. In addition, the subarray overlapping is allowed for the symmetry-based method in contrast with the estimators in [10, 12].

To avoid the high computational cost due to the spectral peak search embedded in [8], we propose an improvement of the approach by using search-free rooting procedure introduced in [9, 10]. In the following, we begin the discussion with a brief review of [8].

#### 3.1.1. Spectral peak search-based algorithm

We decompose the signal space  $\mathbf{U}_s$  into  $\mathbf{U}_{s1}$  and  $\mathbf{U}_{s2}$  by

$$\mathbf{U}_s = \begin{bmatrix} \mathbf{U}_{s1} \\ \text{last } 2M+1-L \text{ rows} \end{bmatrix} = \begin{bmatrix} \text{first } 2M+1-L \text{ rows} \\ \mathbf{U}_{s2} \end{bmatrix}. \quad (18)$$

From the signal model in (7) and the covariance matrix in (16) and (17), it is obvious that there exists a  $K \times K$  full-rank matrix  $\mathbf{G}$  satisfying  $\mathbf{U}_s = \mathbf{A}\mathbf{G}$ .

Similarly,  $\mathbf{U}_{s1}$  and  $\mathbf{U}_{s2}$  corresponding to the first and second subarrays satisfy

$$\begin{aligned} \mathbf{U}_{s1} &= \mathbf{A}_1\mathbf{G}, \\ \mathbf{U}_{s2} &= \mathbf{A}_2\mathbf{G}. \end{aligned} \quad (19)$$

According to the generalized ESPRIT method proposed in [9], we introduce a diagonal matrix

$$\Psi(\theta) = \text{diag}[e^{-j(4\pi d/\lambda)(M-L+1) \sin \theta}, \dots, e^{-j(4\pi d/\lambda)M \sin \theta}]. \quad (20)$$

And for the matrix  $\mathbf{U}_{s2} - \Psi(\theta)(\mathbf{J}\mathbf{U}_{s1})$

$$\begin{aligned} &\mathbf{U}_{s2} - \Psi(\theta)(\mathbf{J}\mathbf{U}_{s1}) \\ &= [\dots, (\mathbf{D}(\theta_k) - \Psi(\theta))(\mathbf{J}\mathbf{a}_1(r_k, \theta_k)), \dots]\mathbf{G}, \end{aligned} \quad (21)$$

the  $k$ th column becomes zero when  $\theta = \theta_k$ , which implies that the rank of matrix  $\mathbf{U}_{s2} - \Psi(\theta)(\mathbf{J}\mathbf{U}_{s1})$  equals  $K-1$ .

The spectrum function

$$P_E(\theta) = \frac{1}{\det[\mathbf{U}_{s2}^H\mathbf{U}_{s2} - \mathbf{U}_{s2}^H\Psi(\theta)(\mathbf{J}\mathbf{U}_{s1})]} \quad (22)$$

is employed to estimate the angles [8]. Obviously, peaks of the spectrum function  $P_E(\theta)$  indicate the estimated angles  $\hat{\theta}_k, k = 1, \dots, K$ .

To avoid aliasing phenomenon due to the periodicity of the exponential function in  $\Psi(\theta)$ , the interelement distance of the ULA should satisfy  $d < (\lambda/4)$ .

#### 3.1.2. Improved search-free algorithm

The bearing estimator (22) involves a high-cost spectral search over the angle  $\theta$ . Observing that the diagonal elements

of the steering diagonal matrix in (20) are proportional to  $e^{-j(4\pi d/\lambda) \sin \theta}$ , we develop a search-free estimator by denoting  $z = e^{-j(4\pi d/\lambda) \sin \theta}$ . We can rewrite (20) as

$$\Psi(z) = \text{diag}[z^{(M-L+1)}, \dots, z^M]. \quad (23)$$

From the above-mentioned property of (21), it is obvious that

$$\det[\mathbf{U}_{s2}^H \mathbf{U}_{s2} - \mathbf{U}_{s2}^H \Psi(z) (\mathbf{J}\mathbf{U}_{s1})] = 0 \quad \text{for } z = e^{-j(4\pi d/\lambda) \sin \theta_k}. \quad (24)$$

The determinant in the left side of (24) returns to a  $L^K$ -order polynomial with respect to  $z$ . The coefficients of this polynomial can be found mathematically from (24), however, it is complicated to give the analytical formulations (not presented here). Obviously, there are totally  $L^K$  roots of (24), however, only  $K$  roots  $\beta_1, \dots, \beta_K$  of them satisfy

$$\text{abs}(\beta_k) = 1. \quad (25)$$

These  $K$  roots indicate the  $K$  estimated directions. In practice, we choose the  $K$  roots closest to the unit circle for estimating the angles of the  $K$  sources. The estimated bearings are obtained by

$$\hat{\theta}_k = \arcsin\left(-\frac{\lambda}{4\pi d} \arg(\beta_k)\right). \quad (26)$$

We note that the diagonal elements of  $\Psi(z)$  are not symmetric. Unlike classical root-MUSIC and root-RARE in [10], the roots of this polynomial do not appear in pairs.

### 3.2. Focusing-based algorithm

In this section, we propose a focusing-based technique to separate the estimation of bearing and that of range.

#### 3.2.1. Focusing technique

We observe that first term of the phase elements in (8) are proportional to  $(2\pi d/\lambda) \sin \theta_k$ , and in addition, it contains only the directions of the source. By using focusing technique [11], the second term can be approximately eliminated, which allows the application of far-field DOA algorithms due to the proportional property of the first term. Focusing technique is developed in [11] for the DOA estimation of far-field wide-band sources, however, we propose to apply this technique to solve a near-field localization problem.

We suppose two different cases: the particular case, where all the sources are closely located; and the general case, where the sources are well separately located.

##### Particular case

The  $K$  sources are located closely in this case. The phase shift function (6) can be rewritten as

$$\tau_{mk} = \left(-\frac{2\pi d}{\lambda} \sin \theta_k\right) m + g(r_k, \theta_k, m), \quad (27)$$

where  $g(r_k, \theta_k, m)$  consists of the second and higher orders of the Taylor expansion for  $\tau_{mk}$ . We have approximately the relation for closely located sources

$$g(r_1, \theta_1, m) - g(r_k, \theta_k, m) \approx 0 \quad \text{for } k = 1, 2, \dots, K. \quad (28)$$

We note that the approximation (28) is true when the DOAs of the sources are small angles. Otherwise, when the angles  $\theta_k$  are big angles, that is,  $|\theta_k| \gg 0$ ,  $g(r_k, \theta_k, m)$  is smaller than the first order property of the Taylor expansion in (27), so (28) is an acceptable approximation for the calculation over  $\tau_{mk}$ .

Then we suppose  $(r_e, \theta_e)$  to be the estimate of these  $K$  closely-located sources obtained from the beamforming-based pre-estimation. Similarly to (28), there is an quasi-equality between  $g(r_e, \theta_e, m)$  and  $g(r_k, \theta_k, m)$  for  $k = 1, 2, \dots, K$ .

We form a diagonal focusing matrix  $\mathbf{B} \in C^{(2M+1) \times (2M+1)}$  by

$$\mathbf{B} = \text{diag}[e^{-jg(r_e, \theta_e, -M)}, \dots, e^{-jg(r_e, \theta_e, M)}], \quad (29)$$

where the function  $g(r_e, \theta_e, m)$  can be obtained from (2) with  $(r_e, \theta_e)$ .

Applying focusing to the covariance matrix  $\mathbf{R}_x$  gives

$$\mathbf{R}_y = \mathbf{B}(\mathbf{A}\mathbf{R}_s\mathbf{A}^H + \sigma^2\mathbf{I})\mathbf{B}^H = \mathbf{B}\mathbf{A}\mathbf{R}_s\mathbf{A}^H\mathbf{B}^H + \sigma^2\mathbf{I}. \quad (30)$$

We can rewrite (30) as

$$\mathbf{R}_y = \mathbf{C}\mathbf{R}_s\mathbf{C}^H + \sigma^2\mathbf{I}, \quad (31)$$

with

$$\mathbf{C} = \mathbf{B}\mathbf{A} = [\mathbf{B}\mathbf{a}(r_1, \theta_1), \dots, \mathbf{B}\mathbf{a}(r_K, \theta_K)]. \quad (32)$$

$\mathbf{C}$  is the focused array manifold matrix. From the approximation (28), we can make the simplification on its  $k$ th column

$$\begin{aligned} \mathbf{c}_k &= \mathbf{B}\mathbf{a}(r_k, \theta_k) \\ &= \begin{bmatrix} e^{j((2\pi d/\lambda) \sin \theta_k)M + jg(r_k, \theta_k, -M) - jg(r_e, \theta_e, -M)} \\ \vdots \\ e^{j(-(2\pi d/\lambda) \sin \theta_k)M + jg(r_k, \theta_k, M) - jg(r_e, \theta_e, M)} \end{bmatrix} \\ &\approx \begin{bmatrix} e^{j((2\pi d/\lambda) \sin \theta_k)M} \\ \vdots \\ e^{j(-(2\pi d/\lambda) \sin \theta_k)M} \end{bmatrix}. \end{aligned} \quad (33)$$

We observe that the focused covariance matrix  $\mathbf{R}_y$  has the same structure as the covariance matrix obtained in far-field situation. The far-field DOA-finding methods are consequently applicable for the bearing estimation.

##### General case

In this case, the  $K$  sources may be separately distributed. In order to employ focusing technique to remove the near-field terms in (8), we assume that the  $K$  sources are located in

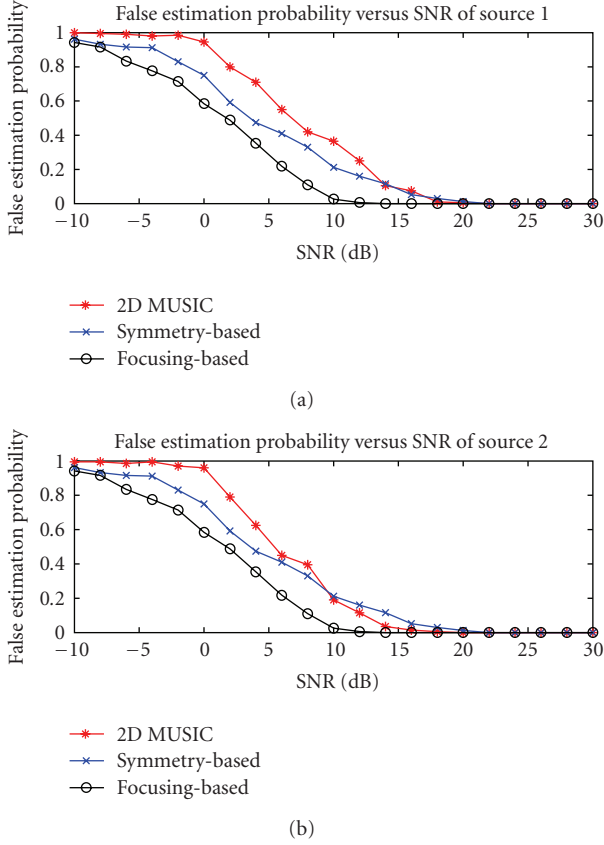


FIGURE 2: False estimation rate versus SNR.

$Q$  different subareas with  $Q < K$  and the total number of sources in  $q$ th subarea is  $P_q$ . Apparently, we have

$$K = \sum_{q=1}^Q P_q. \quad (34)$$

We suppose that  $(r_{e1}, \theta_{e1}), \dots, (r_{eQ}, \theta_{eQ})$  are the  $Q$  estimated sources position obtained from the beamforming-based pre-estimation. Obviously, all the  $P_q$  sources in the  $q$ th subarea are approximately close to one another, that is

$$g(r_{eq}, \theta_{eq}, m) - g(r_{p_q}, \theta_{p_q}, m) \approx 0 \quad \text{for } p_q = 1, 2, \dots, P_q, \quad (35)$$

where  $(r_{p_q}, \theta_{p_q})$  is the position of the  $p$ th source in  $q$ th subarea.

With the assumption (35), we can apply focusing technique to the  $Q$  subareas separately to develop a partially far-field structure of the focused covariance matrix. We note that when focusing on the  $q$ th subarea, only the  $P_q$  estimates inside the subarea could be taken into account.

### 3.2.2. ESPRIT for bearing estimation

The eigen decomposition of the focused array covariance matrix yields

$$\mathbf{R}_y = \mathbf{U}'_s \mathbf{\Lambda}'_s \mathbf{U}'_s{}^H + \mathbf{U}'_n \mathbf{\Lambda}'_n \mathbf{U}'_n{}^H, \quad (36)$$

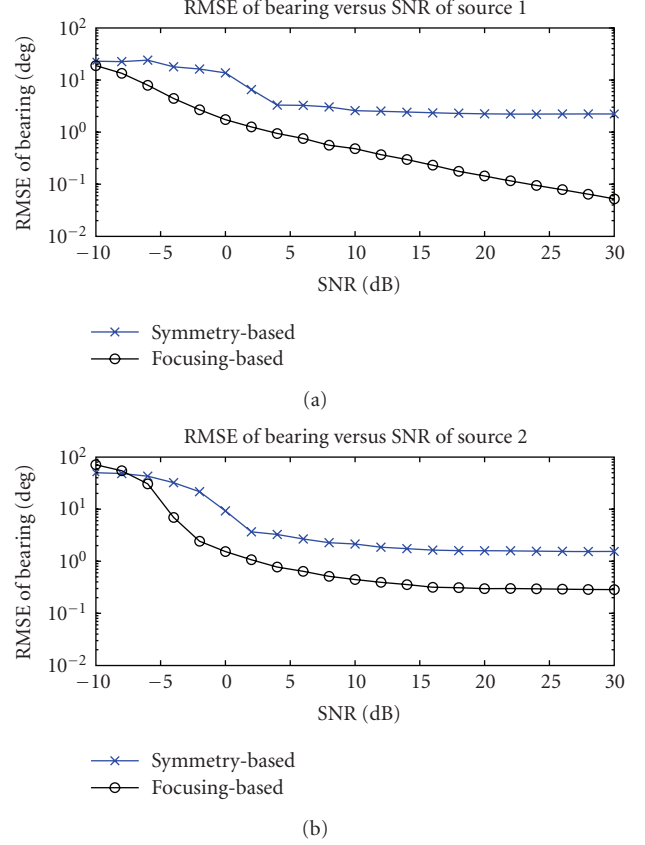


FIGURE 3: RMSE of bearing estimation versus SNR.

where  $\mathbf{U}'_s \in \mathbb{C}^{(2M+1) \times K}$  contains  $K$  eigenvectors spanning the signal subspace of  $\mathbf{R}_y$ , and the diagonal matrix  $\mathbf{\Lambda}'_s \in \mathbb{C}^{K \times K}$  contains the corresponding eigenvalues. Similarly,  $\mathbf{U}'_n \in \mathbb{C}^{(2M+1) \times (2M+1-K)}$  contains  $2M + 1 - K$  eigenvectors in the noise subspace of  $\mathbf{R}_y$ , and the diagonal matrix  $\mathbf{\Lambda}'_n \in \mathbb{C}^{(2M+1-K) \times (2M+1-K)}$  contains the corresponding eigenvalues.

From (17), (31), and (36), we have

$$\mathbf{R}_y = \mathbf{B}(\mathbf{U}_s \mathbf{\Lambda}_s \mathbf{U}_s^H) \mathbf{B}^H + \mathbf{B}(\mathbf{U}_n \mathbf{\Lambda}_n \mathbf{U}_n^H) \mathbf{B}^H, \quad (37)$$

which implies

$$\begin{aligned} \mathbf{U}'_s &= \mathbf{B} \mathbf{U}_s, \\ \mathbf{U}'_n &= \mathbf{B} \mathbf{U}_n. \end{aligned} \quad (38)$$

We divide the ULA into two  $2M$ -element subarrays (from sensor  $-M$  to sensor  $M - 1$  and from sensor  $-M + 1$  to sensor  $M$ ). The focused array manifold matrices for the two subarrays  $\mathbf{C}_1$  and  $\mathbf{C}_2$  can be expressed as

$$\mathbf{C} = \begin{bmatrix} \mathbf{C}_1 \\ \text{last row} \end{bmatrix} = \begin{bmatrix} \text{first row} \\ \mathbf{C}_2 \end{bmatrix}. \quad (39)$$

$\mathbf{U}'_s$  is then similarly partitioned as

$$\mathbf{U}'_s = \begin{bmatrix} \mathbf{U}'_{s1} \\ \text{last row} \end{bmatrix} = \begin{bmatrix} \text{first row} \\ \mathbf{U}'_{s2} \end{bmatrix}. \quad (40)$$

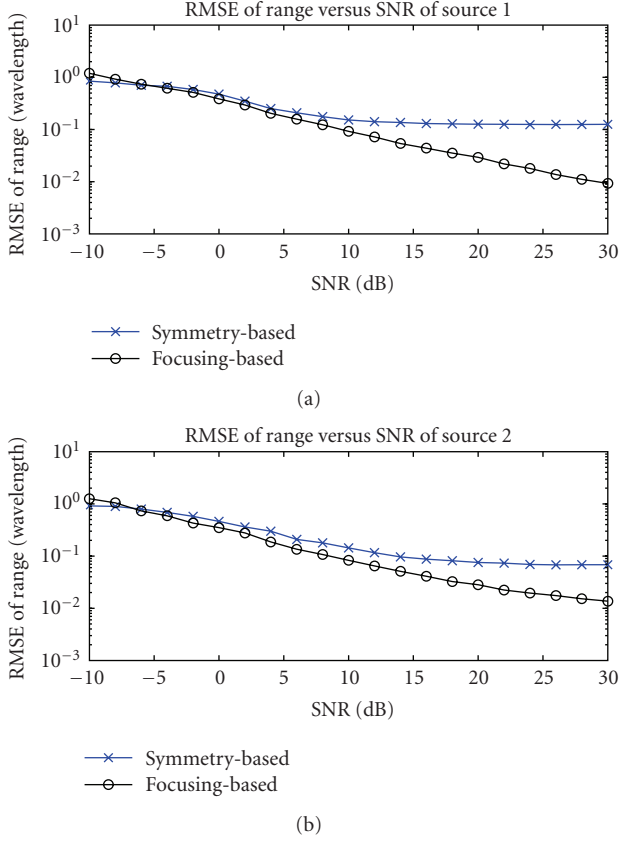


FIGURE 4: RMSE of range estimation versus SNR.

Obviously, there exists a  $K \times K$  full-rank matrix  $\mathbf{V}$  satisfying  $\mathbf{U}'_s = \mathbf{C}\mathbf{V}$ . Hence,  $\mathbf{U}'_{s1}$  and  $\mathbf{U}'_{s2}$  corresponding to the first and second subarray satisfy

$$\begin{aligned} \mathbf{U}'_{s1} &= \mathbf{C}_1\mathbf{V}, \\ \mathbf{U}'_{s2} &= \mathbf{C}_2\mathbf{V}. \end{aligned} \quad (41)$$

From (33), we find that the phase elements of  $\mathbf{c}_k$  are proportional to  $(2\pi d/\lambda) \sin \theta_k$ . Thus,  $\mathbf{C}_1$  and  $\mathbf{C}_2$  satisfy

$$\mathbf{C}_1 = \mathbf{C}_2\Phi, \quad (42)$$

with

$$\Phi = \text{diag}[e^{j((2\pi d/\lambda) \sin \theta_1)}, \dots, e^{j((2\pi d/\lambda) \sin \theta_K)}]. \quad (43)$$

Consequently, we have

$$\mathbf{U}'_{s1} = \mathbf{U}'_{s2}\mathbf{V}^{-1}\Phi\mathbf{V} = \mathbf{U}'_{s2}\Psi. \quad (44)$$

Obviously, the matrix  $\Phi$  has the same eigenvalues as the matrix  $\Psi$  and

$$\Psi = (\mathbf{U}'_{s2H}\mathbf{U}'_{s2})^{-1}\mathbf{U}'_{s2H}\mathbf{U}'_{s1}. \quad (45)$$

Finally, the estimated bearings are obtained by

$$\hat{\theta}_k = \arcsin\left(\frac{\lambda}{2\pi d} \arg(\text{eigenvalues of } \Psi)\right). \quad (46)$$

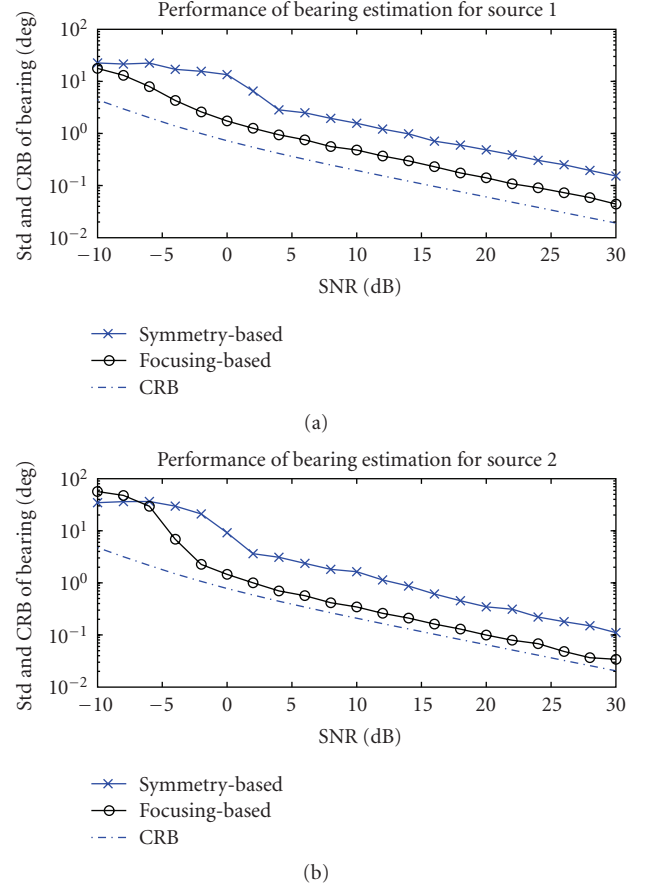


FIGURE 5: Standard deviation and CRB versus SNR of the bearing estimation.

#### 4. RANGE ESTIMATION BY 1D MUSIC METHOD

The range estimation is obtained by maximizing the MUSIC spectrum

$$\hat{r}_k = \arg \max [P_{\text{MUSIC}}^{(k)}(r)], \quad (47)$$

where the MUSIC spectrum is obtained by

$$P_{\text{MUSIC}}^{(k)}(r) = \frac{1}{\mathbf{a}^H(r, \hat{\theta}_k) \mathbf{U}_n \mathbf{U}_n^H \mathbf{a}(r, \hat{\theta}_k)}. \quad (48)$$

To avoid the parameter pairing, we form the MUSIC spectrum for each estimated bearing.

#### 5. SIMULATION RESULTS

In this section, Monte Carlo simulations are implemented to test the resolution and the estimation efficiency of the algorithms.

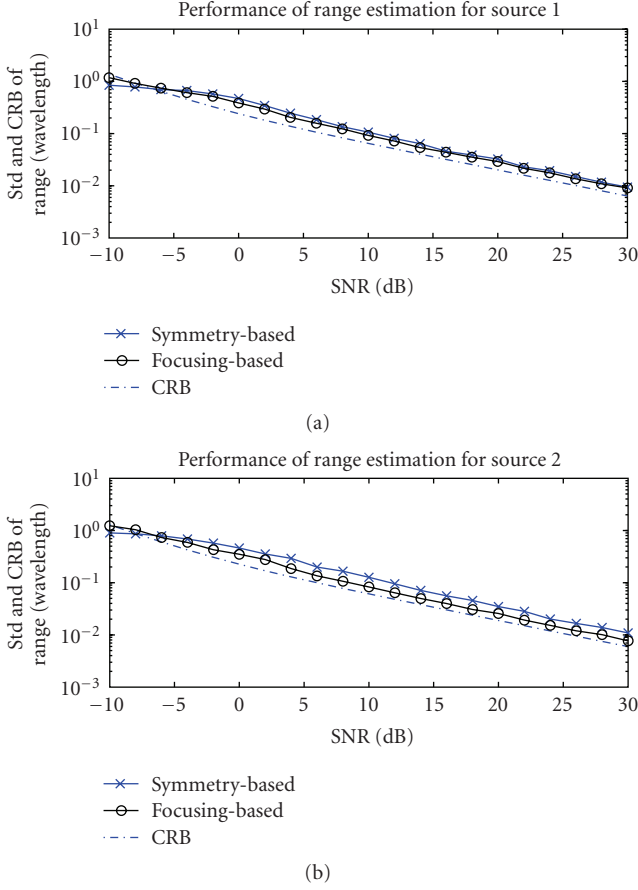


FIGURE 6: Standard deviation and CRB versus SNR of the range estimation.

### 5.1. False estimation rate comparison

To test the resolution performance of these two algorithms, we introduce the false estimation probability defined by the following equation:

$$P_e = \frac{N_e}{N} = \frac{\text{Number of false estimates}}{\text{Number of estimates}}. \quad (49)$$

We suppose an estimate of the  $K$  sources to be  $[(\hat{r}_1, \hat{\theta}_1), \dots, (\hat{r}_K, \hat{\theta}_K)]$ . If the estimates of all the  $K$  sources satisfy

$$\begin{aligned} |\hat{r}_k - r_k| &\leq \epsilon_r \quad \text{for } k = 1, 2, \dots, K, \\ |\hat{\theta}_k - \theta_k| &\leq \epsilon_\theta \quad \text{for } k = 1, 2, \dots, K, \end{aligned} \quad (50)$$

the corresponding estimate is considered to be a good estimate, otherwise it is a false estimate.  $\epsilon_r$  and  $\epsilon_\theta$  in above equations are the tolerant error for the range estimation and for bearing estimation, respectively.

We simulate first a simple case in which a symmetric ULA with  $M = 4$  (i.e., the number of sensors equals 9) and  $d = \lambda/5$  is employed to localize two uncorrelated narrow-band sources located at  $(r_1, \theta_1) = (4.2\lambda, 15^\circ)$  and  $(r_2, \theta_2) = (3.8\lambda, 25^\circ)$ . The error tolerance is set as  $\epsilon_r = 0.2\lambda$  for range and  $\epsilon_\theta = 5^\circ$  for bearing. 200 independent trials are performed

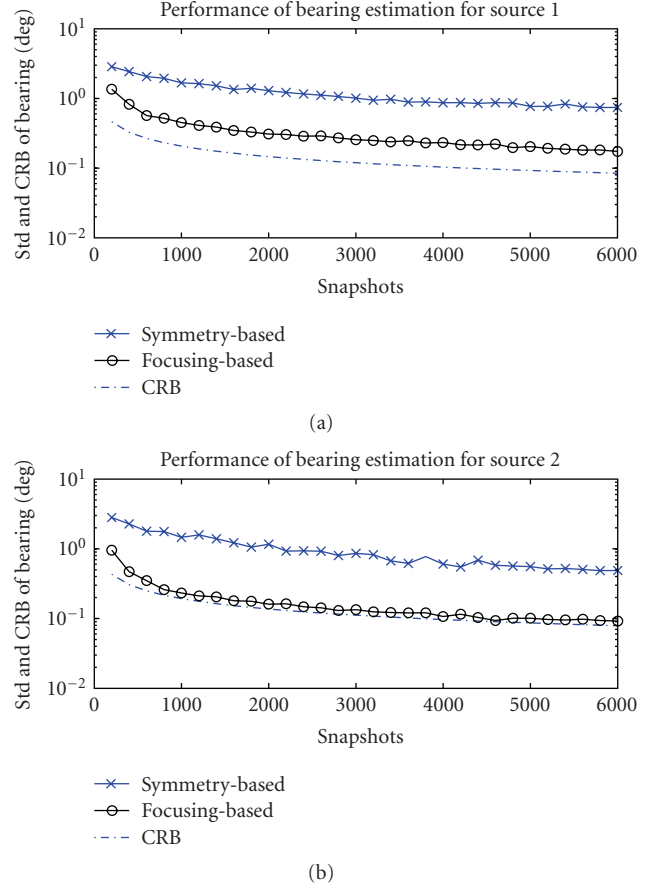


FIGURE 7: Standard deviation and CRB versus snapshots of the bearing estimation.

at different SNRs with 1000 snapshots. Figure 2 shows the false estimation probability of these two methods compared with that of 2D MUSIC method.

The solid lines marked by stars in the figure indicate the false estimation probability of 2D MUSIC method. The lines with x-mark signify the false estimation probability of the symmetry-based method, and the lines with circle figure out the false estimation probability of the focusing-based method. From Figure 2, we find that the focusing-based method has a better performance compared to the other two methods. This is because the focusing-based method utilizes the a priori information from the pre-estimation.

### 5.2. Root mean square error comparison

The RMSEs of estimates from the symmetry-based method and focusing-based method obtained in Section 5.1 have been presented in this part. Figures 3 and 4 illustrate the RMSE of estimated parameter from the algorithms.

The lines with x-mark signify the RMSE of the estimated parameters from the symmetry-based method, and the lines with circles indicate the RMSE of the estimated parameters from the focusing-based method. From Figures 3 and 4, we find that there exists small biases for these two estimators. This is because the approximations have been used as we

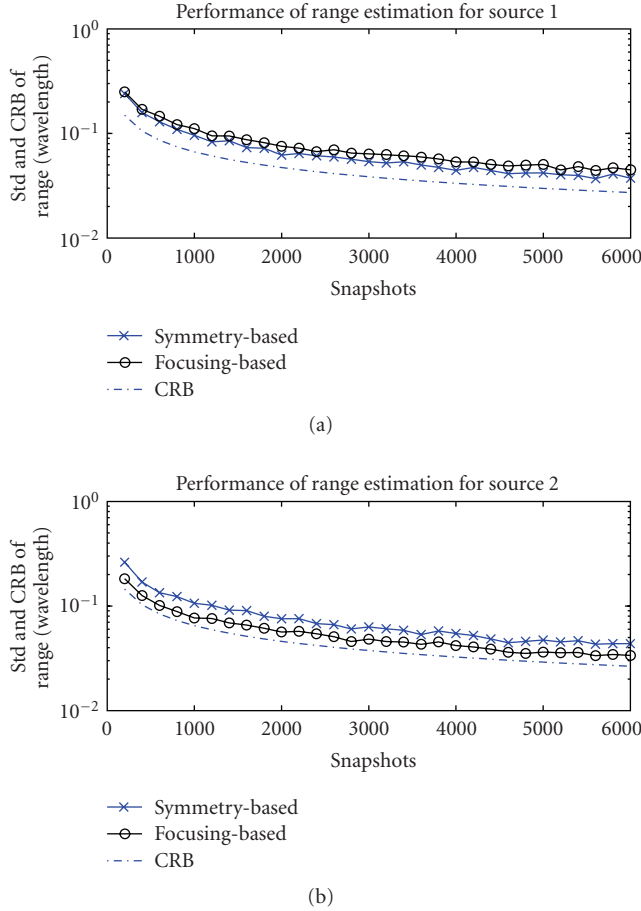


FIGURE 8: Standard deviation and CRB versus snapshots of the range estimation.

have introduced previously. Obviously, the biases from the symmetry-based method are comparatively greater than those from the focusing-based method.

### 5.3. Standard deviation comparison

In this part, the standard deviation of the estimates from these two methods are compared with the corresponding Crammer-Rao Bound (CRB) given in [6]. 200 Monte Carlo simulations are performed at different SNRs (from  $-10$  dB to  $30$  dB) and with different numbers of snapshots (from 200 to 6000). 1000 snapshots are used for the comparison versus SNRs, and SNR is  $10$  dB in the comparison versus numbers of snapshots. The other simulation parameters are the same as we have used in Section 5.1.

Figures 5 and 6 illustrate the standard deviation of the estimated bearing and range versus SNR, respectively. The solid lines signed by circles in these figures indicate the estimated parameters from the focusing-based method, and the lines with x-mark indicate the estimated parameters from the symmetry-based method. The dash-dot lines indicate the square roots of the corresponding CRBs. The lines with x-mark signify the false estimation probability of the symmetry-based method, and the lines with circle figure

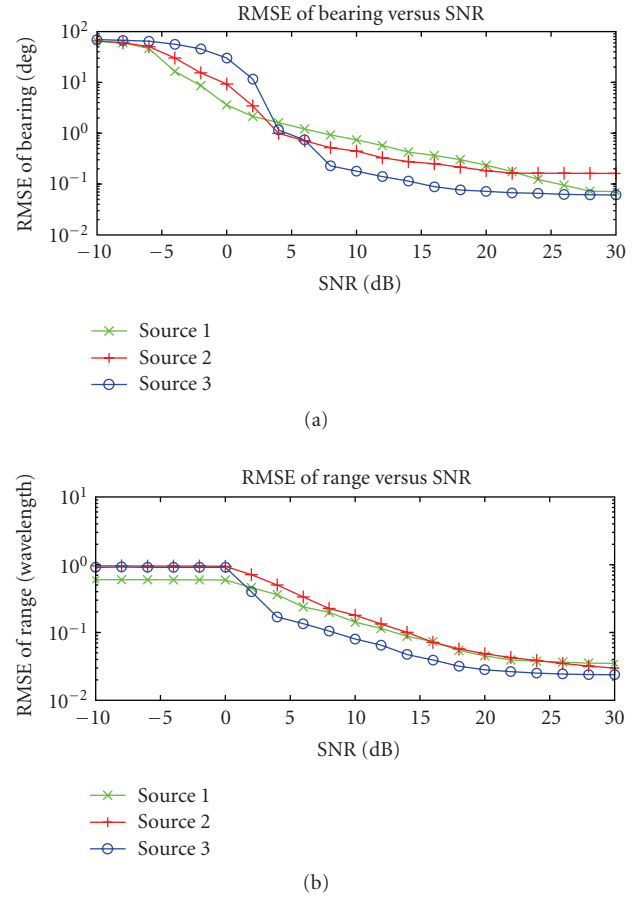


FIGURE 9: Performance of focusing-based method for separated sources.

out the false estimation probability of the focusing-based method. Obviously, the focusing-based estimator is more efficient than the symmetry-based estimator.

Similarly, Figures 7 and 8 display the bearing and range estimation versus numbers of snapshots, respectively.

### 5.4. Well-separated sources

To test the focusing-based method in case of well-separated sources, we simulate another scenario of the localization of 3 sources located at  $(r_1, \theta_1) = (4.2\lambda, 15^\circ)$ ,  $(r_2, \theta_2) = (4\lambda, 25^\circ)$ , and  $(r_3, \theta_3) = (3\lambda, -15^\circ)$  with the previous array. The RMSEs of the 500 independent estimates from focusing-based algorithm under different SNRs (from  $-10$  dB to  $30$  dB) are illustrated in Figure 9. 1000 snapshots are used in this simulation.

We find that the estimator has a better performance on the source  $(r_3, \theta_3)$ . This is because when we focus on the subarea around source  $(r_3, \theta_3)$ , the interference from source  $(r_1, \theta_1)$  and  $(r_2, \theta_2)$  is not significant due to the large spading between source  $(r_3, \theta_3)$  and source  $(r_1, \theta_1)$  and  $(r_2, \theta_2)$ . While the symmetry-based estimator fails to separate the 3 sources (the results are not presented here).

## 6. CONCLUSION

This paper discusses two fast algorithms with high-resolution performance for 2D near-field multiple sources localization. The symmetry-based method is improved and a focusing-based method is proposed. By applying a search-free procedure, the symmetry-based algorithm requires no longer spectral peak search for bearing estimation; while the focusing technique is employed to the near-field received signal model in order to obtain a far-field structure which allows the application of far-field DOA algorithms for bearing estimation. 1D MUSIC method is applied to estimate the range of each source with the estimated bearing. Unlike other algorithms for near-field source localization, the algorithms can localize multiple sources in the near field without high-cost multidimensional search, high-order statistics or parameter pairing.

## REFERENCES

- [1] J.-F. Chen, X.-L. Zhu, and X.-D. Zhang, "A new algorithm for joint range-DOA-frequency estimation of near-field sources," *EURASIP Journal on Applied Signal Processing*, vol. 2004, no. 3, pp. 386–392, 2004.
- [2] P. Stoica and A. Nehorai, "MUSIC, maximum likelihood, and Cramer-Rao bound," *IEEE Transactions on Acoustics, Speech, and Signal Processing*, vol. 37, no. 5, pp. 720–741, 1989.
- [3] J. C. Chen, R. E. Hudson, and K. Yao, "Maximum-likelihood source localization and unknown sensor location estimation for wideband signals in the near-field," *IEEE Transactions on Signal Processing*, vol. 50, no. 8, pp. 1843–1854, 2002.
- [4] Y.-D. Huang and M. Barkat, "Near-field multiple source localization by passive sensor array," *IEEE Transactions on Antennas and Propagation*, vol. 39, no. 7, pp. 968–975, 1991.
- [5] H. Chuberre, T. Filleul, and J.-J. Fuchs, "Near-field sources localization: a model-fitting approach," in *Proceedings of IEEE International Conference on Acoustics, Speech and Signal Processing (ICASSP '95)*, vol. 5, pp. 3555–3558, Detroit, Mich, USA, May 1995.
- [6] E. Grosicki, K. Abed-Meraim, and Y. Hua, "A weighted linear prediction method for near-field source localization," *IEEE Transactions on Signal Processing*, vol. 53, no. 10, part 1, pp. 3651–3660, 2005.
- [7] N. Yuen and B. Friedlander, "Performance analysis of higher order ESPRIT for localization of near-field sources," *IEEE Transactions on Signal Processing*, vol. 46, no. 3, pp. 709–719, 1998.
- [8] W. Zhi and M. Y.-W. Chia, "Near-field source localization via symmetric subarrays," *IEEE Signal Processing Letters*, vol. 14, no. 6, pp. 409–412, 2007.
- [9] F. Gao and A. B. Gershman, "A generalized ESPRIT approach to direction-of-arrival estimation," *IEEE Signal Processing Letters*, vol. 12, no. 3, pp. 254–257, 2005.
- [10] M. Pesavento, A. B. Gershman, and K. M. Wong, "Direction finding in partly calibrated sensor arrays composed of multiple subarrays," *IEEE Transactions on Signal Processing*, vol. 50, no. 9, pp. 2103–2115, 2002.
- [11] S. Marcos, *Les Méthodes à haute résolution: Traitement d'antenne et analyse spectrale*, Hermès, Paris, France, 1998.
- [12] C. M. S. See and A. B. Gershman, "Direction-of-arrival estimation in partly calibrated subarray-based sensor arrays," *IEEE Transactions on Signal Processing*, vol. 52, no. 2, pp. 329–338, 2004.